Two-Dimensional Linear Homeomorphic Oculomotor Plant Mathematical Model

Oleg V. Komogortsev, *Member, IEEE*, Corey Holland, Sampath Jayarathna, *Student Member, IEEE*
Department of Computer Science, Texas State University – San Marcos, TX 78666-4616, USA
ok11@txstate.edu, ch1570@txstate.edu, sampath@txstate.edu

Abstract – This paper builds a two-dimensional linear homeomorphic oculomotor plant mathematical model and assesses its ability to simulate person-specific oblique saccades on a two-dimensional plane. The proposed model is driven by a simplified pulse-step neuronal control signal and accounts in a linear form for the unique characteristics of the eye globe and the extraocular muscles responsible for horizontal and vertical rotation (the lateral/medial recti and superior/inferior recti respectively). These characteristics include: series elasticity, length tension, passive elasticity, viscosity, eye globe inertial mass, and the force-velocity relationships of agonist/antagonist muscles. Results indicate that the model is capable of producing oblique saccade trajectories with properties resembling those of normal humans. The model can be simplified into two one-dimensional models for quicker signal simulation, making it applicable for time sensitive applications. Practical applications of the model might include: enhanced security in biometric identification systems; improved noise reduction and signal recovery facilities for eye tracking systems; and additional metrics from which to determine user effort during usability testing.

Index Terms – Oculomotor plant, model, simulation, prediction, human visual system, saccade

I. INTRODUCTION

THE HUMAN OCULOMOTOR PLANT (OP) consists of the eye globe and six extraocular muscles (medial rectus, lateral rectus, superior rectus, inferior rectus, superior oblique, and inferior oblique). The OP, driven by the neuronal control signal, exhibits six primary eye movement types: fixations, saccades, smooth pursuits, optokinetic reflex, vestibular-ocular reflex, and vergence [1]. Each extraocular muscle (EOM) is represented by a complex anatomical structure consisting of components that can be considered abstractly through such properties as elasticity, viscosity, active state tension, length tension, and force-velocity relationships. The human eye globe rotates in three degrees of freedom with eye movements following Listing's and Donders' Laws [2].

There are two primary categories of OP models that have been presented to the scientific community thus far. The first of these categories consists of the one-dimensional, generally linear, models developed by Westheimer [3], Robinson [4], Clark and Stark [5], Bahill [6], Komogortsev and Khan [7, 8], Enderle and Zhou [9], and Martin and Schovanec [10]. The model developed by Westheimer represented the OP as a linear second order system. Robinson's model added the pulse-step neuronal control mechanics with the OP system presented as a fourth order system. Neither model was capable of producing trajectories consistent with the main sequence relationship and normal human data. Bahill developed a sixth order linear homeomorphic OP model driven by a simplified pulse-step neuronal control signal, with velocity output close to the physiological recordings of normal humans; however, Bahill's model generated only rightward saccades from the primary eye position. Komogortsev and Khan modified Bahill's model, providing the capability of generating both rightward and leftward saccades from any angular position. The OP developed by Enderle and Zhou extends Bahill's model with an additional characteristics related to the neuronal control signal and the plant itself. The OP model developed by Martin and Schovanec is a non-linear tenth order system, which employs a more anatomically accurate hill-type individual extraocular muscle model with passive elasticity modeled in a non-linear fashion.

The second category consists of three-dimensional, generally non-linear, OP models capable of simulating eye movement trajectories in 3D space. These models can be broken into two subcategories. The first being those OP models which do not employ the individual anatomical properties of each EOM [11-13], and the second being those that do [14, 15]. The OP models of the latter group are non-linear and provide the most accurate representation of anatomical components, such as the individual properties of the extraocular muscles and pulley mechanics. Quaia and Optican [16] present a good overview of these models.

The two-dimensional oculomotor plant mathematical model (2D-OP) presented in this paper builds on the horizontal OP model created by Komogortsev and Khan [7, 8], and provides the ability to simulate saccade trajectories given the coordinates of the saccade's onset and offset position. The 2D-OP incorporates several important characteristics of the human oculomotor plant. Each extraocular muscle is modeled individually, maintaining the physiological agonist-antagonist nature of extraocular movement dynamics. The model of each muscle encapsulates the series elasticity, length tension, viscosity, active state tension, and force-velocity relationship properties by creating a linear mathematical representation of each component. The model is driven by a simplified pulse-step neuronal control signal, sent by the brain to the extraocular muscles. For normal humans, the duration of saccades is linearly dependent on their amplitude [17], and

an exponential relationship between the maximum velocity of saccades and their amplitude is maintained, often referred to as the main sequence relationship [1, 18, 19]. The proposed model assumes linear dependency between the amplitude of a saccade and its duration, and is evaluated in terms of positional accuracy and its ability to maintain a realistic main sequence relationship. In this work we assume that oculomotor plant characteristics (OPC) are unique for each individual.

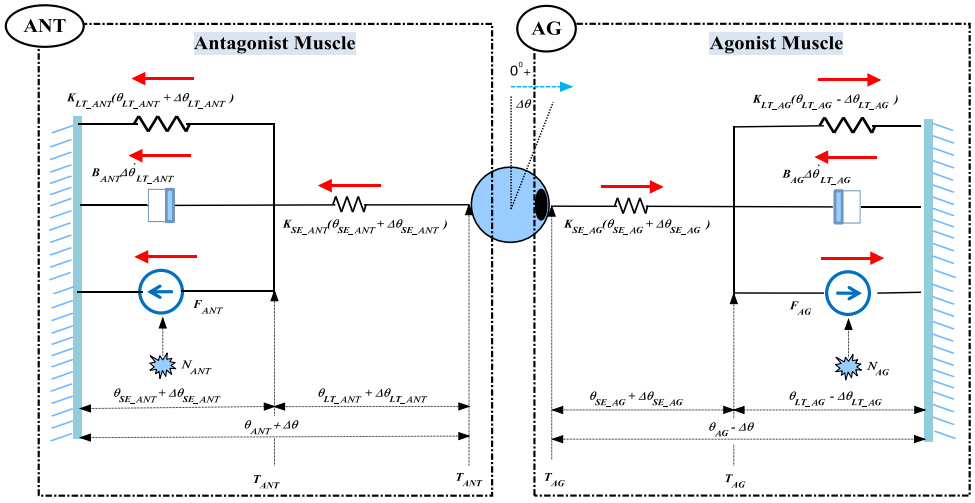

Figure 1. 1D-OP: Right eye. Rightward horizontal rotation performed by the medial rectus (agonist) and lateral rectus (antagonist). AG and ANT mark agonist and antagonist parts of the diagram correspondingly. The diagram contains agonist and antagonist specific presentation of the K_{se} and K_{lt} but, corresponding equations are presented without the AG and ANT subscript to avoid cluttering.

To the best of our knowledge, there is no previous research that investigates the applicability of a linear homeomorphic representation of the OP for the simulation of oblique saccades. Such a representation would be particularly useful for its speed, analytic tractability, and acceptable accuracy for applications that employ eye movements in the domains of human-computer interaction, biometrics, eye tracking, and usability. A preliminary version of the 2D-OP presented here was discussed in [20], however our previous work but did not provide the mathematical equations for all directions of movement on the 2D plane and did not verify the model's simulation accuracy against recorded data. This paper resolves these issues. An additional contribution of this work is the collection and analysis of oblique saccade data from a relatively large subject pool.

Paper structure: Section II provides an overview of the human oculomotor system including a brief description of the oculomotor plant and basic eye movements. Section III presents the equations describing the 2D-OP. Section IV presents the methodology employed for acquisition of the human eye movement data, and provides the details of OPC parameter estimation. Section V presents evaluation results. Sections VI and VII present a discussion of the results.

II. HUMAN OCULOMOTOR SYSTEM

The eye globe is rotated by six extraocular muscles (EOM), with each EOM being driven by a neuronal control signal generated by the brain. The role of each EOM can be represented by the following table [1].

INDIVIDUAL EXTRAOCULAR MUSCLE ROLES

Muscle	Primary	Secondary	Tertiary
Lateral rectus (LR)	Abduction	N/A	N/A
Medial rectus (MR)	Adduction	N/A	N/A
Inferior rectus (IR)	Depression	Extortion	Adduction
Superior rectus (SR)	Elevation	Intortion	Adduction
Inferior oblique (IO)	Extortion	Elevation	Abduction
Superior oblique (SO)	Intorsion	Depression	Abduction

The neuronal control signals for the horizontal and vertical components of eye movements are generated by different parts of the brain. Specifically, the premotor neurons in the pons and medulla are responsible for horizontal eye movements, and the rostral midbrain is responsible for vertical eye movements. The roles of the individual EOMs can be defined as agonist (subscript notation AG), the EOM that pulls the eye globe in the required direction, or antagonist (subscript notation ANT), the EOM that resists the pull.

A. Extraocular Muscle Structure

Each muscle is represented by a complex anatomical structure [21], and has a multitude of characteristics, including: ***active state tension*** – tension developed as a result of muscle innervation by the neuronal control signal; ***length tension relationship*** – the relationship between the length of a muscle and the force it is capable of exerting for a given innervation; ***force-velocity relationship*** – the relationship between the velocity of a muscle extension/contraction and the force it is capable of exerting; ***passive elasticity*** – the resisting properties of a muscle not innervated by the neuronal control signal; ***series elasticity*** – resistive properties of a muscle while the muscle is innervated by the neuronal control signal. More detailed descriptions of these characteristics can be found in [6]. As well, aside from the individual muscle properties, the eye globe has passive elastic and viscous characteristics due to the properties of the surrounding tissues.

B. Human Saccade Characteristics

The OP, driven by the neuronal control signal, exhibits six eye movement types: fixations, saccades, smooth pursuits, optokinetic reflex, vestibulo-ocular reflex, and vergence [1], however for the purposes of this work only saccades are considered.

Saccades occur when the eye globe rotates very quickly between points of eye fixation, and saccade amplitude refers

to the difference, in degrees of the visual angle, from the point of pre-saccade fixation to the point of post-saccade fixation, where the central eye position represents the origin; e.g., a purely horizontal saccade made from 10° right of center with an amplitude of -15° would reposition the eye to 5° left of center. Saccades of given amplitude produced by an individual tend to show similarities in a number of properties, including: reaction time, duration, position, velocity, acceleration, and waveform. As well, certain relationships exist between saccades of varying amplitudes, these include: the amplitude-peak velocity relationship, the amplitude-duration relationship, and the velocity waveform.

The amplitude-peak velocity relationship, also referred to as the main sequence relationship [18], describes the tendency for saccadic peak velocity to increase in an exponential manner until saturation begins to occur at a certain velocity maximum (V_{MAX}), according to the following formula:

$$V_{PEAK} = V_{MAX}(1 - \exp\left(-\frac{|Amplitude|}{C}\right)) \quad \textbf{(1)}$$

The amplitude-duration relationship describes the tendency for saccade duration to increase linearly with saccade amplitude from a certain base duration (D_{MIN}) according to the formula:

$$D = D_{MIN} + C|Amplitude| \quad \textbf{(2)}$$

Both the main sequence and amplitude-duration relationship vary for different angles of motion; that is, purely horizontal/vertical saccades and oblique saccades of different angles exhibit different relationships. While there has been considerable research into these relationships as they relate to purely horizontal/vertical saccades [1], there is relatively little information on oblique saccades [19]. As well, these relationships have been noted to vary between individuals and may be affected by subject age [22, 23], recording medium [24], and initial eye position [25].

The velocity waveform is another characteristic that remains similar across saccades of varying amplitudes. The skewness of the waveform can be estimated from the ratio of the time to reach maximum velocity to the total duration of the saccade, and varies from roughly 0.5 for small saccades to 0.2 for large saccades. Similarly, it has been noted that the ratio of peak velocity to average velocity (Q) remains nearly constant at 1.6 for horizontal/vertical saccades of all amplitudes [1].

Given the fact that the horizontal and vertical components of human saccades are generated by separate areas of the brain and display noted differences in duration and peak velocity, oblique trajectories should be curved when component durations are unequal. While this is true for a substantial percentage of oblique saccades, a similarly substantial percentage exhibit trajectories that are nearly straight, more so than could be explained by the random synchronization of component durations [26].

Based on the frequent occurrence of straight oblique trajectories, it is apparent that the neural signals responsible for the horizontal and vertical components of oblique saccades in some way influence each other. Whether component stretching occurs before or after generation of the neuronal control signal is an area of active research [27]. To simplify the analysis of our model, we assume that the duration of both components of movement are equal.

III. OCULOMOTOR PLANT MATHEMATICAL MODEL

A. Agonist EOM Model

The AG part of Figure 1 demonstrates the forces involved when the agonist muscle pulls the eye globe in the direction of displacement Δθ. The agonist muscle is innervated by the neuronal control signal N_{AG}, contracts, rotates the eye globe, and stretches the antagonist muscle. A detailed description of muscle dynamics during innervation is presented in [28].

Using Figure 1, we can write the equation of force with which the part of the diagram responsible for contraction (active state tension, damping components, length tension component) pulls the series elasticity component:

$$T_{AG} = F_{AG} + K_{LT}(\theta_{LT\_AG} - \Delta\theta_{LT\_AG}) - B_{AG}\Delta\dot{\theta}_{LT\_AG} \quad \textbf{(3)}$$

Resisting the contraction, the series elasticity component propagates the contractile force by pulling the eye globe with the same force T_{AG}.

$$T_{AG} = K_{SE}(\theta_{SE\_AG} + \Delta\theta_{SE\_AG}) \quad \textbf{(4)}$$

Equations (3) and (4) can be rearranged to move the contribution from length tension (θ_{LT_AG}) and series elasticity (θ_{SE_AG}) components to the modified active state tension ($\hat{F}_{AG}$) and damping components ($\hat{B}_{AG}$). This transition makes it possible to present the force equations with a variable depicting eye globe rotation Δθ. Details of this calculation are presented in [29]. It should be noted that the passive properties of the EOMs are combined with the orbital tissue properties for simplicity.

$$\hat{T}_{AG} = \frac{\hat{F}_{AG}K_{SE}}{K_{SE} + K_{LT}} - \frac{\Delta\theta K_{SE}K_{LT}}{K_{SE} + K_{LT}} - \hat{B}_{AG}\Delta\dot{\theta}_{LT\_AG} \quad \textbf{(5)}$$

$$\hat{T}_{AG} = K_{SE}(\Delta\theta_{LT\_AG} - \Delta\theta) \quad \textbf{(6)}$$

B. Antagonist EOM Model

The ANT part of Figure 1 demonstrates the forces involved when the antagonist muscle is stretched in the direction of eye globe displacement Δθ. The antagonist muscle is innervated by the neuronal control signal N_{ANT} and becomes stretched by the pull of the agonist muscle.

Using Figure 1, we can write the equation of force with which the part of the diagram responsible for contraction (active state tension, damping components, length tension component) pulls the series elasticity component:

$$T_{ANT} = -F_{ANT} - K_{LT}(\theta_{LT\_ANT} - \Delta\theta_{LT\_ANT}) - B_{ANT}\Delta\dot{\theta}_{LT\_ANT} \quad \textbf{(7)}$$

Resisting the contraction, the series elasticity component propagates the contractile force by pulling the eye globe with the same force T_{AG}.

$$T_{ANT} = K_{SE}(\theta_{SE\_ANT} + \Delta\theta_{SE\_ANT}) \quad \textbf{(8)}$$

Equations (7) and (8) can be used to calculate the force T_{ANT} in terms of eye globe rotation Δθ, and displacement $\Delta\theta_{LT\_ANT}$ in the length tension component of the muscle.

Again, the passive properties of the EOMs are combined with the orbital tissue properties for simplicity.

$$\hat{T}_{ANT} = -\frac{\hat{F}_{ANT}K_{SE}}{K_{SE}+K_{LT}} - \frac{\Delta\theta K_{SE}K_{LT}}{K_{SE}+K_{LT}} - \hat{B}_{ANT}\Delta\dot{\theta}_{LT\_ANT} \quad \textbf{(9)}$$

$$\hat{T}_{ANT} = -K_{SE}(\Delta\theta - \Delta\theta_{LT\_ANT}) \quad \textbf{(10)}$$

C. Pulse-Step Neuronal Control

The neuronal control signal is represented as neuronal discharge from the brain, with discharge frequency determining the neuronal innervation of an EOM [30]. Different approaches are employed for the representation of the neuronal control signal sent by the brain to the EOMs. Simplified approaches describe the signal as a pulse-step function where the pulse part of the signal relates in some fashion to the amplitude of the simulated saccades [6, 8]. More sophisticated approaches such as the one presented by Enderle and Zhou [9] break the pulse part of the signal into several pieces and employs additional low pass filtering mechanisms on top of the pulse-step form to provide a more realistic representation of the neuronal signal. An approach developed by Goldstein and Robinson [31] and Optican and Miles [32] described the neuronal control signal as being generated by a pulse-slide-step function, in which the agonist neural pulse is recalculated continuously throughout the saccade producing an exponential decay (slide) to the post-saccade step. Both sophisticated approaches described above require recorded saccade trajectory to infer neuronal control signal parameters, i.e., saccade simulation where only onset and offset parameters are provided for trajectory simulation becomes more complex than in the simplified pulse-step approach.

In this paper, we employ a simplified pulse-step form, because it requires less parameters than other forms and allows for an easy trajectory simulation given the onset and offset coordinates of the simulated saccades.

The step part of the signal is created by the positional command (angular eye position prior to and immediately after a saccade), and the pulse part of the signal is created by the velocity command, which is determined by the amplitude of the programmed saccade.

$$N_{AG\_SAC}(t) = \begin{cases} N_{AG\_SAC\_ONSET}, t_{SAC\_ONSET} \le t < t_{AG\_SAC\_PULSE\_START} \\ N_{AG\_SAC\_PULSE}, t_{AG\_SAC\_PULSE\_START} \le t < t_{AG\_SAC\_PULSE\_END} \\ N_{AG\_SAC\_OFFSET}, t_{AG\_SAC\_PULSE\_END} \le t < t_{SAC\_OFFSET} \end{cases}$$

$$N_{ANT\_SAC}(t) = \begin{cases} N_{ANT\_SAC\_ONSET}, t_{SAC\_ONSET} \le t < t_{ANT\_SAC\_PULSE\_START} \\ N_{ANT\_SAC\_PULSE}, t_{ANT\_SAC\_PULSE\_START} \le t < t_{ANT\_SAC\_PULSE\_END} \\ N_{ANT\_SAC\_OFFSET}, t_{ANT\_SAC\_PULSE\_END} \le t < t_{SAC\_OFFSET} \end{cases}$$

t_{NAME} constants present time parameters for each type of muscle and action phase. t is the time elapsed from the beginning of the saccade. The quantity $t_{AG\_SAC\_PULSE\_END} - t_{AG\_SAC\_PULSE\_START}$ refers to the width of the pulse (PW_{AG}) in the agonist EOM and is expressed in the following form, where $\theta_{SAC\_OFFSET} - \theta_{SAC\_ONSET}$ represents the amplitude of the simulated saccade, p_1 and p_2 are constants:

$$PW_{AG} = p_1|\theta_{SAC\_OFFSET} - \theta_{SAC\_ONSET}| + p_2 \quad \textbf{(11)}$$

The antagonist pulse circumscribes the agonist pulse by 3 ms on either side [6], starting 3 ms before the agonist pulse and ending 3 ms after, hence: $PW_{ANT} = PW_{AG} + 6$.

Assuming that the eye movement type before and after the simulated saccade is a fixation, the equations for the neuronal control signal for the onset and offset of a saccade can be written as follows:

$$N_{AG\_SAC\_ONSET}(\theta_{SAC\_ONSET}) = \begin{cases} N_{AG\_FIX}(\theta_{SAC\_ONSET}), if\ AG\ before \\ N_{ANT\_FIX}(\theta_{SAC\_ONSET}), if\ ANT\ before \end{cases}$$

$$N_{AG\_SAC\_OFFSET}(\theta_{SAC\_OFFET}) = \begin{cases} N_{AG\_FIX}(\theta_{SAC\_OFFSET}), if\ AG\ after \\ N_{ANT\_FIX}(\theta_{SAC\_OFFSET}), if\ ANT\ after \end{cases}$$

$$N_{ANT\_SAC\_ONSET}(\theta_{SAC\_ONSET}) = \begin{cases} N_{AG\_FIX}(\theta_{SAC\_ONSET}), if\ AG\ before \\ N_{ANT\_FIX}(\theta_{SAC\_ONSET}), if\ ANT\ before \end{cases}$$

$$N_{ANT\_SAC\_OFFSET}(\theta_{SAC\_OFFET}) = \begin{cases} N_{AG\_FIX}(\theta_{SAC\_OFFSET}), if\ AG\ after \\ N_{ANT\_FIX}(\theta_{SAC\_OFFSET}), if\ ANT\ after \end{cases}$$

$N_{AG\_FIX}(\theta)$ and $N_{ANT\_FIX}(\theta)$ are represented in the following form [8]:

$$N_{AG\_FIX}(\Delta\theta) = N_{FIX\_C} + N_{AG\_C}|\Delta\theta| \quad \textbf{(12)}$$

$$N_{ANT\_FIX}(\Delta\theta) = N_{FIX\_C} - N_{ANT\_C}|\Delta\theta| \quad \textbf{(13)}$$

We have empirically selected an exponential function to determine the strength of the agonist neural pulse as a function of saccade amplitude, were $\theta_{SAC\_OFFSET} - \theta_{SAC\_ONSET}$ represents the amplitude of the simulated saccade, p_3 and p_4 are constants, and $N_{ANT\_SAC\_PULSE}$ is a constant of 0.5.

$$N_{AG\_SAC\_PULSE} = p_3\left(1 - e^{|\theta_{SAC\_OFFSET} - \theta_{SAC\_ONSET}|/p_4}\right) \quad \textbf{(14)}$$

D. Transformation of the Neural Signal to Muscle Tension

While the change in the discharge frequency specified by the pulse-step neuronal control signal is instantaneous, the change in the active state tension and EOM forces is not.

The active state tension of the agonist and the antagonist go through a low pass filtering process, and can be modeled by the following equations, where τ_{AG} and τ_{ANT} are functions that define the low pass filtering process [6]:

$$\hat{F}_{AG}(t) = \frac{N_{AG} - \hat{F}_{AG}(t)}{\tau_{AG}} \quad \textbf{(15)}$$

$$\hat{F}_{ANT}(t) = \frac{N_{ANT} - \hat{F}_{ANT}(t)}{\tau_{ANT}} \quad \textbf{(16)}$$

$$\tau_{AG}(t) = \begin{cases} \tau_{AG\_DE}, t_{SAC\_ONSET} \le t < t_{AG\_SAC\_START} \\ \tau_{AG\_AC}, t_{AG\_SAC\_START} \le t < t_{AG\_SAC\_END} \\ \tau_{AG\_DE}, t_{AG\_SAC\_END} \le t < t_{SAC\_OFFSET} \end{cases}$$

$$\tau_{ANT}(t) = \begin{cases} \tau_{ANT\_DE}, t_{SAC\_ONSET} \le t < t_{ANT\_SAC\_START} \\ \tau_{ANT\_AC}, t_{ANT\_SAC\_START} \le t < t_{ANT\_SAC\_END} \\ \tau_{ANT\_DE}, t_{ANT\_SAC\_END} \le t < t_{SAC\_OFFSET} \end{cases}$$

τ_{AG_AC}, τ_{AG_DE}, τ_{ANT_AC}, τ_{ANT_DE} are activation/deactivation time constants that define the low pass filtering process.

E. 1D Oculomotor Plant Mathematical Model (1D-OP)

The equations for the one dimensional case, e.g. horizontal movement, are created by considering all forces that contribute to the rotation of the eye globe.

The agonist force dynamics can be described by combining equations (5) and (6):

$$K_{SE}(\Delta\theta_{LT\_AG} - \Delta\theta) = \frac{\hat{F}_{AG}K_{SE}}{K_{SE}+K_{LT}} - \frac{\Delta\theta K_{SE}K_{LT}}{K_{SE}+K_{LT}} - \hat{B}_{AG}\Delta\dot{\theta}_{LT\_AG} \quad \textbf{(17)}$$

Antagonist dynamics are derived by combining equations (9) and (10):

$$K_{SE}(\Delta\theta - \Delta\theta_{LT\_ANT}) = \frac{\hat{F}_{ANT}K_{SE}}{K_{SE}+K_{LT}} + \frac{\Delta\theta K_{SE}K_{LT}}{K_{SE}+K_{LT}} + \hat{B}_{ANT}\Delta\dot{\theta}_{LT\_ANT} \quad \textbf{(18)}$$

Newton's second law is applied to connect the equations for acceleration and inertia to all forces acting on the eye globe:

$$J\Delta\ddot{\theta} = \hat{T}_{AG} + \hat{T}_{ANT} + K_P\Delta\theta + B_P\Delta\dot{\theta} \quad \textbf{(19)}$$

T_{AG} is the force applied by the agonist muscle to the eye globe, T_{ANT} is the force applied by the antagonist muscle to the eye globe, $K_p\Delta\theta$ is a linear spring representing the passive elastic properties of the EOMs and the eye globe, $B_p\Delta\dot{\theta}$ is a damping component representing the viscous properties of the eye orbit and surrounding tissues.

Equations (15) and (16) describe the dynamics of the active state tension, and the last equation connects the derivative of position to the velocity of the movement signal:

$$\Delta\dot{\theta} = \Delta\dot{\theta} \quad \textbf{(20)}$$

These six differential equations, (15)-(20), can be represented in matrix form with the following variables creating a state vector: $x_1(k) = \Delta\theta$ – eye rotation, $x_2(k) = \Delta\theta_{LT\_AG}$ and $x_3(k) = \Delta\theta_{LT\_ANT}$ – displacement of the length tension component, $x_4(k) = \Delta\dot{\theta}$ – eye velocity, $x_5(k) = \hat{F}_{AG}$ and $x_6(k) = \hat{F}_{ANT}$ active state tension (for the agonist and antagonist EOMs respectively). Then:

$$\dot{x} = Ax + u \quad \textbf{(21)}$$

where x is a 1 × 6 state vector, A is a 6 × 6 transition matrix, and u is a 1 × 6 control vector. The transition matrix A and control vector u change depending on the direction of movement.

Positive Direction Movements:

During movements in the positive direction (e.g. right eye is rotating rightward), the transition matrix and control vector are as follows:

$$\begin{pmatrix} 1 & 0 & 0 & \Delta\rho & 0 & 0 \\ \Delta\rho\frac{K_{SE}^2}{(K_{LT}+K_{SE})\hat{B}_{AG}} & \left(1-\Delta\rho\frac{K_{SE}}{\hat{B}_{AG}}\right) & 0 & 0 & \Delta\rho\frac{K_{SE}}{(K_{LT}+K_{SE})\hat{B}_{AG}} & 0 \\ \Delta\rho\frac{K_{SE}^2}{(K_{LT}+K_{SE})\hat{B}_{ANT}} & 0 & \left(1-\Delta\rho\frac{K_{SE}}{\hat{B}_{ANT}}\right) & 0 & 0 & -\Delta\rho\frac{K_{SE}}{(K_{LT}+K_{SE})\hat{B}_{ANT}} \\ -\Delta\rho\frac{2K_{SE}+K_p}{J} & \Delta\rho\frac{K_{SE}}{J} & \Delta\rho\frac{K_{SE}}{J} & 1-\Delta\rho\frac{B_p}{J} & 0 & 0 \\ 0 & 0 & 0 & 0 & \left(1-\frac{\Delta\rho}{\tau_{AG}}\right) & 0 \\ 0 & 0 & 0 & 0 & 0 & \left(1-\frac{\Delta\rho}{\tau_{ANT}}\right) \end{pmatrix}$$

$$u = \begin{bmatrix} 0 & 0 & 0 & 0 & \frac{\Delta\rho}{\tau_{AG}}N_{AG\_SAC} & \frac{\Delta\rho}{\tau_{ANT}}N_{ANT\_SAC} \end{bmatrix}^T \quad \textbf{(22)}$$

Negative Direction Movements:

During movements in the negative direction (e.g. right eye is rotating leftward), the transition matrix and control vector are as follows:

$$\begin{pmatrix} 1 & 0 & 0 & \Delta\rho & 0 & 0 \\ \Delta\rho\frac{K_{SE}^2}{(K_{LT}+K_{SE})\hat{B}_{AG}} & \left(1-\Delta\rho\frac{K_{SE}}{\hat{B}_{AG}}\right) & 0 & 0 & \Delta\rho\frac{K_{SE}}{(K_{LT}+K_{SE})\hat{B}_{ANT}} & 0 \\ \Delta\rho\frac{K_{SE}^2}{(K_{LT}+K_{SE})\hat{B}_{ANT}} & 0 & \left(1-\Delta\rho\frac{K_{SE}}{\hat{B}_{ANT}}\right) & 0 & 0 & -\Delta\rho\frac{K_{SE}}{(K_{LT}+K_{SE})\hat{B}_{AG}} \\ \Delta\rho\frac{2K_{SE}+K_p}{J} & \Delta\rho\frac{K_{SE}}{J} & \Delta\rho\frac{K_{SE}}{J} & 1-\Delta\rho\frac{B_p}{J} & 0 & 0 \\ 0 & 0 & 0 & 0 & \left(1-\frac{\Delta\rho}{\tau_{ANT}}\right) & 0 \\ 0 & 0 & 0 & 0 & 0 & \left(1-\frac{\Delta\rho}{\tau_{AG}}\right) \end{pmatrix}$$

$$u = \begin{bmatrix} 0 & 0 & 0 & 0 & \frac{\Delta\rho}{\tau_{ANT}}N_{ANT\_SAC} & \frac{\Delta\rho}{\tau_{AG}}N_{AG\_SAC} \end{bmatrix}^T \quad \textbf{(23)}$$

As a result, equation (21) completely describes the 1D-OP during horizontal saccades. A more detailed description of the 1D-OP can be found in [7, 29].

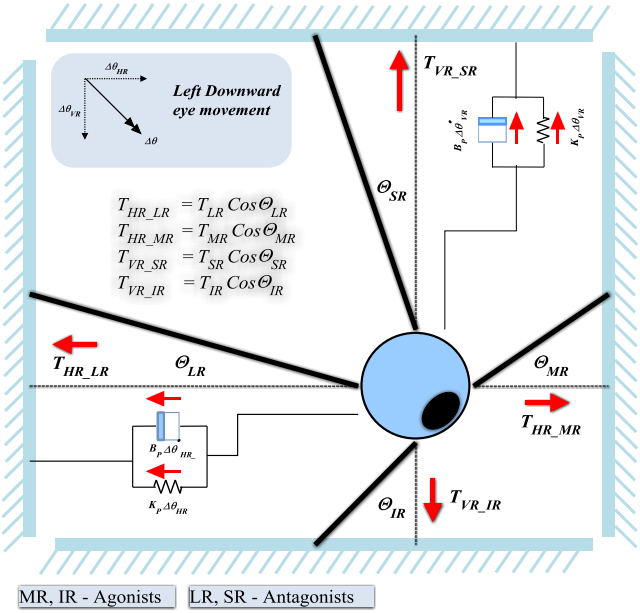

Figure 2. 2D-OP: Right eye, front view. Left downward eye movement performed by medial and inferior recti as agonists, and lateral and superior recti as antagonists. EOMs are presented as single black lines.

F. 2D Oculomotor Plant Mathematical Model (2D-OP)

One of the objectives of the 2D-OP presented in this paper is to accurately simulate saccade trajectories on the 2D plane. According to Table I, the rotation of the eye globe with a mapped gaze position on a 2D plane can be primarily attributed to four EOMs – the lateral, medial, superior, and inferior recti. Figure 2 depicts the four EOM forces (T_{LR}, T_{MR}, T_{SR}, and T_{IR}) responsible for left-downward rotation of the eye globe.

During 2D rotation, the movement dynamics and roles of the EOMs remain essentially the same as in 1D rotation. The agonist muscles contract and pull the eye globe in the required direction and the antagonist muscles stretch and resist the pull.

Twelve differential equations describe the 2D-OP. Two equations are created as a result of the application of Newton's second law to the vertical and horizontal components of the eye movement. Four equations describe the dynamics of the EOM forces that move the eye globe. The horizontal (HR) component of movement is conducted by the forces created by the lateral (T_{HR_LR}) and medial (T_{HR_MR}) recti. The vertical (VR) component of movement is conducted by the forces created by the superior (T_{VR_SR}) and inferior (T_{VR_IR}) recti. Four equations describe the transformation of the neuronal control signal in each EOM to the active state tension following the mechanism described in Section III.E. Two equations connect the velocity of the eye movement to the position of the eye in the vertical and horizontal planes.

The derivation of all equations, except the four equations describing the dynamics of the EOM forces, in general, follows the mechanics described in the previous subsections. To provide better analytical tractability of the dynamics of the EOM forces, the following sections present a description

of the forces for all possible scenarios of rotation: right-upward, left-upward, right-downward, and left-downward. The derivation of the 2D-OP equations is presented in [28].

G. Left-Downward Rotation

The EOM forces responsible for rotation of the eye globe can be found as projections to the horizontal and vertical axis. Figure 2 illustrates this case.

During left-downward movement of the right eye (saccade between two fixation points) with amplitude of $\Delta\theta$ the medial recuts and inferior rectus as agonists move the eye to its destination, stretching the antagonist EOMs (the lateral and superior recti). $\Delta\theta_{HR}$ and $\Delta\theta_{VR}$ represent the horizontal and vertical components of eye globe rotation, measured in degrees. All EOMs in the 2D-OP become tilted to a set of new angles Θ_{LR}, Θ_{MR}, Θ_{SR}, and Θ_{IR} in regard to the primary eye globe position.

The medial and inferior recti are agonists, while the lateral and superior recti are antagonists.

$$K_{SE}(\Delta\theta_{HR} - \Delta\theta_{HR\_LT\_LR}) = \frac{\hat{F}_{LR}K_{SE}}{K_{SE}+K_{LT}} + \frac{\Delta\theta_{HR}K_{SE}}{K_{SE}+K_{LT}} + \hat{B}_{ANT}\Delta\dot{\theta}_{HR\_LT\_LR} \quad \textbf{(24)}$$

$$K_{SE}(\Delta\theta_{HR\_LT\_MR} - \Delta\theta_{HR}) = \frac{\hat{F}_{MR}K_{SE}}{K_{SE}+K_{LT}} - \frac{\Delta\theta_{HR}K_{SE}K_{LT}}{K_{SE}+K_{LT}} - \hat{B}_{AG}\Delta\dot{\theta}_{HR\_LT\_MR} \quad \textbf{(25)}$$

$$K_{SE}(\Delta\theta_{VR} - \Delta\theta_{VR\_LT\_SR}) = -\frac{\hat{F}_{IR}K_{SE}}{K_{SE}+K_{LT}} + \frac{\Delta\theta_{VR}K_{SE}K_{LT}}{K_{SE}+K_{LT}} + \hat{B}_{AG}\Delta\dot{\theta}_{VR\_LT\_IR} \quad \textbf{(26)}$$

$$K_{SE}(\Delta\theta_{VR} - \Delta\theta_{VR\_LT\_SR}) = \frac{\hat{F}_{SR}K_{SE}}{K_{SE}+K_{LT}} + \frac{\Delta\theta_{VR}K_{SE}K_{LT}}{K_{SE}+K_{LT}} + \hat{B}_{ANT}\Delta\dot{\theta}_{VR\_LT\_SR} \quad \textbf{(27)}$$

Application of Newton's second law to the horizontal and vertical component of movement yields:

$$J\Delta\ddot{\theta}_{HR} = T_{HR\_MR} - T_{HR\_LR} - K_p\Delta\theta_{HR} - B_p\Delta\dot{\theta}_{HR} \quad \textbf{(28)}$$

$$J\Delta\ddot{\theta}_{HR} = -K_{SE}(\Delta\theta_{HR\_LT\_MR} - \Delta\theta_{HR}) - K_{SE}(\Delta\theta_{HR} - \Delta\theta_{HR\_LT\_LR}) - K_p\Delta\theta_{HR} - B_p\Delta\dot{\theta}_{HR} \quad \textbf{(29)}$$

where J represents the eye globe's inertial mass, $\Delta\theta_{HR}$ represents the horizontal rotation of the eye, $\Delta\dot{\theta}_{HR}$ represents the horizontal velocity of eye rotation, and $\Delta\ddot{\theta}_{HR}$ represents the horizontal acceleration.

For the vertical component of movement, the following equation can be written:

$$J\Delta\ddot{\theta}_{VR} = -K_{SE}(\Delta\theta_{VR\_LT\_IR} - \Delta\theta_{VR}) - K_{SE}(\Delta\theta_{VR} - \Delta\theta_{VR\_LT\_SR}) - K_p\Delta\theta_{VR} - B_p\Delta\dot{\theta}_{VR} \quad \textbf{(30)}$$

The forces represented by equations (29) and (30) are identical for all directions of movement, and therefore are not described in later subsections.

H. Right-Upward Rotation

The lateral and superior recti are agonists, while the medial and inferior recti are antagonists.

$$K_{SE}(\Delta\theta_{HR\_LT\_LR} - \Delta\theta_{HR}) = \frac{\hat{F}_{LR}K_{SE}}{K_{SE}+K_{LT}} - \frac{\Delta\theta_{HR}K_{SE}}{K_{SE}+K_{LT}} - \hat{B}_{AG}\Delta\dot{\theta}_{HR\_LT\_LR} \quad \textbf{(31)}$$

$$K_{SE}(\Delta\theta_{HR} - \Delta\theta_{HR\_LT\_MR}) = \frac{\hat{F}_{MR}K_{SE}}{K_{SE}+K_{LT}} + \frac{\Delta\theta_{HR}K_{SE}}{K_{SE}+K_{LT}} + \hat{B}_{ANT}\Delta\dot{\theta}_{HR\_LT\_MR} \quad \textbf{(32)}$$

$$K_{SE}(\Delta\theta_{VR} - \Delta\theta_{VR\_LT\_IR}) = \frac{\hat{F}_{IR}K_{SE}}{K_{SE}+K_{LT}} + \frac{\Delta\theta_{VR}K_{SE}}{K_{SE}+K_{LT}} + \hat{B}_{ANT}\Delta\dot{\theta}_{VR\_LT\_IR} \quad \textbf{(33)}$$

$$K_{SE}(\Delta\theta_{VR\_LT\_SR} - \Delta\theta_{VR}) = \frac{\hat{F}_{SR}K_{SE}}{K_{SE}+K_{LT}} - \frac{\Delta\theta_{VR}K_{SE}}{K_{SE}+K_{LT}} - \hat{B}_{AG}\Delta\dot{\theta}_{VR\_LT\_SR} \quad \textbf{(34)}$$

I. Left-Upward Rotation

The medial and superior recti are the agonists, while the lateral and inferior recti are the antagonists.

$$K_{SE}(\Delta\theta_{VR\_LT\_SR} - \Delta\theta_{VR}) = \frac{\hat{F}_{SR}K_{SE}}{K_{SE}+K_{LT}} - \frac{\Delta\theta_{VR}K_{SE}}{K_{SE}+K_{LT}} - \hat{B}_{AG}\Delta\dot{\theta}_{VR\_LT\_SR} \quad \textbf{(35)}$$

$$K_{SE}(\Delta\theta_{HR\_LT\_MR} - \Delta\theta_{HR}) = \frac{\hat{F}_{MR}K_{SE}}{K_{SE}+K_{LT}} - \frac{\Delta\theta_{HR}K_{SE}}{K_{SE}+K_{LT}} - \hat{B}_{AG}\Delta\dot{\theta}_{HR\_LT\_MR} \quad \textbf{(36)}$$

$$K_{SE}(\Delta\theta_{VR} - \Delta\theta_{VR\_LT\_IR}) = \frac{\hat{F}_{IR}K_{SE}}{K_{SE}+K_{LT}} + \frac{\Delta\theta_{VR}K_{SE}}{K_{SE}+K_{LT}} + \hat{B}_{ANT}\Delta\dot{\theta}_{VR\_LT\_IR} \quad \textbf{(37)}$$

$$K_{SE}(\Delta\theta_{VR} - \Delta\theta_{VR\_LT\_IR}) = \frac{\hat{F}_{IR}K_{SE}}{K_{SE}+K_{LT}} + \frac{\Delta\theta_{VR}K_{SE}}{K_{SE}+K_{LT}} + \hat{B}_{ANT}\Delta\dot{\theta}_{VR\_LT\_IR} \quad \textbf{(38)}$$

J. Right-Downward Rotation

The lateral and inferior recti are agonists, while the medial and superior recti are antagonists.

$$K_{SE}(\Delta\theta_{HR\_LT\_LR} - \Delta\theta_{HR}) = \frac{\hat{F}_{LR}K_{SE}}{K_{SE}+K_{LT}} - \frac{\Delta\theta_{HR}K_{SE}}{K_{SE}+K_{LT}} - \hat{B}_{AG}\Delta\dot{\theta}_{HR\_LT\_LR} \quad \textbf{(39)}$$

$$-K_{SE}(\Delta\theta_{HR} - \Delta\theta_{HR\_LT\_MR}) = -\frac{\hat{F}_{MR}K_{SE}}{K_{SE}+K_{LT}} \pm \frac{\Delta\theta_{HR}K_{SE}}{K_{SE}+K_{LT}} - \hat{B}_{ANT}\Delta\dot{\theta}_{HR\_LT\_MR} \quad \textbf{(40)}$$

$$K_{SE}(\Delta\theta_{VR\_LT\_IR} - \Delta\theta_{VR}) = \frac{\hat{F}_{IR}K_{SE}}{K_{SE}+K_{LT}} - \frac{\Delta\theta_{VR}K_{SE}}{K_{SE}+K_{LT}} - \hat{B}_{AG}\Delta\dot{\theta}_{VR\_LT\_IR} \quad \textbf{(41)}$$

$$K_{SE}(\Delta\theta_{VR} - \Delta\theta_{VR\_LT\_SR}) = \frac{\hat{F}_{SR}K_{SE}}{K_{SE}+K_{LT}} + \frac{\Delta\theta_{HR}K_{SE}}{K_{SE}+K_{LT}} + \hat{B}_{ANT}\Delta\dot{\theta}_{VR\_LT\_SR} \quad \textbf{(42)}$$

K. Representation of the 2D-OP via two 1D-OP

Force equations represented by (24)-(42) indicate that equations of all forces and for all directions of movement can be separated into only vertical and horizontal components, allowing us to employ the mechanism illustrated by equations (15)-(21) to generate each component of movement separately. The general form of this solution is represented by the following set of equations:

$$\dot{x} = Ax + u \quad \textbf{(43)}$$

$$\dot{y} = By + c \quad \textbf{(44)}$$

where A and B are transition matrices, x and y are state vectors, and u and c are control vectors for the horizontal and vertical components respectively. The choice of the transition matrix and control vector depends on the direction of movement in each of its components. Movements in the positive direction are performed by the transitional matrix and control vector described by (22), and negative direction movements are performed by (23). State vectors are populated by the EOMs responsible for the agonist and antagonist roles.

The reduction of the 12 variable system to two 6 variable sets allows a considerable reduction (up to 4 times) in the overall computational requirements, and provides an opportunity to efficiently utilize multi-core systems for the generation of the 2D-OP eye movement signal.

IV. METHODOLOGY

L. Participants

Eye movement data was collected for a total of 30 subjects (24 males / 6 females), ages 18-40 with an average age of 23 (SD = 5.3). Mean positional accuracy of the recordings averaged between all calibration points was 1.31° (SD = 0.88°). For consistency, only data recorded from the right eye was used in the current paper. Data collection procedures were approved by the Texas State University Institutional Review Board, and all subjects provided informed consent.

M. Apparatus & Software

Eye movements were recorded using an EyeLink II eye tracker [33] running at 1000 Hz, a chinrest was employed to improve eye tracking accuracy, and subjects were positioned such that the primary eye position corresponded to the center of the screen. Stimuli were presented on a flat screen monitor positioned at a distance of roughly 685 millimeters from the subject, with screen dimensions of 640 × 400 millimeters, and resolution of 2560 × 1600 pixels.

All algorithms and data analysis were implemented and performed in MATLAB.

N. Data Collection Procedure

The screen was divided into four Cartesian quadrants, with the center of the screen (and central eye position) as the origin. Eye movement records were generated for participants' centrifugal saccades at different angles within the 1st quadrant (upper-right). Due to the screen dimensions: stimuli of 3°, 6°, 9°, 12°, 15°, and 18° amplitude were presented at oblique angles of 0°, 15°, 30°, 45°, and 60°; stimuli of 3°, 6°, 9°, 12°, and 15° amplitude were presented at oblique angles of 75° and 90°. This resulted in a total of 40 stimulus-evoked oblique saccades per recording, for 1200 saccades across all subjects. A stimulus was presented at the origin before each saccade, and the order of stimulus presentation was randomized for each subject according to a uniform distribution. The stimulus was presented as a white dot of 30 pixels diameter with a smaller black dot of 12 pixels diameter at its center, the background was black, and each stimulus was shown for 1000 ms.

O. Saccade Extraction Process

The raw eye movement records were processed to identify individual points as being part of a fixation or saccade. A velocity threshold algorithm [34] was employed to classify individual points with a velocity greater than 25°/sec as saccades, where all remaining points were assumed to be fixations. Following the initial classification, a micro-saccade filter re-classified saccades with amplitude less than 0.25° as fixations and a micro-fixation filter re-classified fixations with a duration less than 50 milliseconds as saccades.

Algorithm: OPC Estimation
Input: Measured saccade trajectories
Output: Estimated Oculomotor plant characteristics (OPC)

1. Perform optimization of all OPC across all possible pulse widths for each saccade using NM to minimize the absolute positional error between the measured and simulated trajectory. This generates an OPC set for each possible pulse width of each saccade.
2. Select initial 3 least-error OPC sets for each saccade.
3. For each subject, average and fix the least-error values of the following model OPC across all saccades: K_{SE_AG}, K_{SE_ANT}, K_{LT_AG}, K_{LT_ANT}, N_{AG_C}, N_{ANT_C}, B_P, B_{AG}, B_{ANT}, J, τ_{ANT_AC}, τ_{AG_DE}, τ_{ANT_DE}, N_{FIX_C}, N_{ANT_SAC}.
4. Perform optimization on the remaining OPC (τ_{AG_AC}, N_{AG_SAC}) across all possible pulse widths (PW_{AG}) for each saccade using NM to minimize the absolute positional error between the measured and simulated trajectory.
5. Select the 3 least-error OPC subsets for each saccade.
6. For each subject, fix τ_{AG_AC} to the mode of its least-error values.
7. Perform optimization on the remaining OPC (N_{AG_SAC}) across all possible pulse widths (PW_{AG}) for each saccade using NM to minimize the absolute positional error between the measured and simulated trajectory.
8. Select the 3 least-error OPC subsets for each saccade.
9. For each subject, perform exponential regression of the form represented by equation (12) on the values of N_{AG_SAC}.
10. Calculate absolute positional error of the various OPC sets across all possible pulse widths (PW_{AG}) for each saccade.
11. Select the 3 least-error pulse widths for each saccade.
12. Perform linear regression of the form represented by equation (11) on the values of PW_{AG}.

Figure 3. OPC estimation psuedocode.

Stimulus-evoked centrifugal saccades were extracted from the eye movement records according to the following criteria: the saccade occurs between 100 and 500 ms after the stimulus is displayed; the saccade has a duration between 10 and 200 ms; at least one component of the saccade has a positive amplitude. Only centrifugal saccades were considered, as it has been found that centrifugal/centripetal saccades often exhibit different dynamics [25] By filtering saccades in this manner, the algorithm was able to identify an average of 38 (SD = 2.1) stimulus-evoked saccades per recording. Across all subjects, 1140 of the possible 1200 stimulus-evoked saccades were identified.

P. Data Sets

Extracted centrifugal saccades were divided into three groups according to their amplitude. The first group consisted of saccades with amplitudes between 0-10°, the second group of 0-15°, and the third group included all recorded saccades, where the maximum vectorial amplitude was approximately 24°. All saccade groups were employed for the 2D-OP testing.

TABLE I
ESTIMATED OCULOMOTOR PLANT CHARACTERISTICS

	0 – 10° Amplitude				*0 – 15° Amplitude*				*All Saccades*			
	Horizontal		**Vertical**		**Horizontal**		**Vertical**		**Horizontal**		**Vertical**	
Parameter	**μ**	**σ**	**μ**	**σ**	**μ**	**σ**	**μ**	**σ**	**μ**	**σ**	**μ**	**σ**
K_{SE_AG}	2.6	0.3	2.4	0.3	2.5	0.3	2.4	0.2	2.5	0.3	2.3	0.3
K_{SE_ANT}	2.9	0.5	2.7	0.4	2.9	0.4	2.6	0.4	2.9	0.4	2.6	0.4
K_{LT_AG}	1.3	0.1	1.3	0.1	1.3	0.1	1.3	0.1	1.3	0.1	1.3	0.1
K_{LT_ANT}	1.4	0.1	1.4	0.1	1.4	0.1	1.4	0.1	1.4	0.1	1.4	0.1
N_{AG_C}	0.88	0.09	0.86	0.06	0.88	0.08	0.86	0.05	0.88	0.08	0.86	0.04
N_{ANT_C}	0.48	0.03	0.48	0.03	0.48	0.03	0.48	0.03	0.48	0.03	0.48	0.02
B_P	0.044	0.009	0.045	0.009	0.042	0.008	0.043	0.008	0.040	0.007	0.043	0.007
B_{AG}	0.043	0.005	0.045	0.005	0.040	0.004	0.042	0.004	0.040	0.004	0.041	0.004
B_{ANT}	0.017	0.004	0.019	0.003	0.018	0.003	0.019	0.003	0.017	0.003	0.019	0.003
J	$5.0(10^{-5})$	$0.8(10^{-5})$	$5.3(10^{-5})$	$0.7(10^{-5})$	$5.0(10^{-5})$	$0.8(10^{-5})$	$5.4(10^{-5})$	$0.6(10^{-5})$	$4.9(10^{-5})$	$0.8(10^{-5})$	$5.4(10^{-6})$	$0.6(10^{-5})$
τ_{AG_AC}	1.5	0.1	1.5	0.1	1.5	0.0	1.5	0.0	1.5	0.0	1.5	0.0
τ_{ANT_AC}	3.1	0.2	3.0	0.2	3.1	0.2	3.0	0.2	3.1	0.2	3.0	0.2
τ_{AG_DE}	2.4	0.1	2.4	0.1	2.4	0.1	2.4	0.1	2.4	0.1	2.4	0.1
τ_{ANT_DE}	2.0	0.2	2.1	0.2	2.1	0.1	2.2	0.1	2.1	0.1	2.2	0.1
N_{FIX_C}	14.7	1.6	14.1	1.9	15.6	1.6	14.6	1.7	15.9	1.4	14.6	1.6
$N_{AG\_SAC\ PULSE}$ *	$349.6\ (1 - e^{-\lvert A\rvert / 28.4})$		$274.3\ (1 - e^{-\lvert A\rvert / 23.4})$		$175.3\ (1 - e^{-\lvert A\rvert / 17.5})$		$216.4\ (1 - e^{-\lvert A\rvert / 23.6})$		$163.3\ (1 - e^{-\lvert A\rvert / 17.7})$		$144.7\ (1 - e^{-\lvert A\rvert / 13.8})$	
$N_{ANT\_SAC\ PULSE}$	0.52	0.03	0.51	0.03	0.51	0.03	0.51	0.03	0.51	0.02	0.51	0.03
PW_{ANT} *	1.2 |A| + 6.0		1.6 |A| + 5.7		1.6 |A| + 7.4		1.8 |A| + 6.5		1.6 |A| + 9.0		1.8 |A| + 7.0	
p1	1.2	0.7	1.6	0.9	1.6	0.6	1.8	0.7	1.7	0.6	1.7	0.8
p2	6.1	3.4	5.8	2.8	7.3	3.5	6.7	2.1	2.3	4.3	1.6	3.0
p3	$2.6(10^5)$	$3.6(10^5)$	$3.8(10^5)$	$4.0(10^5)$	$1.8(10^5)$	$3.5(10^5)$	$2.9(10^5)$	$4.7(10^5)$	$9.4(10^4)$	$2.4(10^5)$	$2.5(10^5)$	$3.6(10^5)$
p4	$2.1(10^4)$	$2.4(10^4)$	$3.4(10^4)$	$3.5(10^4)$	$1.8(10^4)$	$3.3(10^4)$	$3.5(10^4)$	$5.8(10^4)$	$1.3(10^4)$	$3.3(10^4)$	$3.0(10^4)$	$3.9(10^4)$

* Due to high variability in the values of p1-p4, an additional regression was performed across all subjects to provide a more accurate representation.

TABLE II
POSITIONAL ACCURACY

	0 – 10° Amplitude				*0 – 15° Amplitude*				*All Saccades*			
	RMSE		**R^2**		**RMSE**		**R^2**		**RMSE**		**R^2**	
Component	**μ**	**σ**	**μ**	**σ**	**μ**	**σ**	**μ**	**σ**	**μ**	**σ**	**μ**	**σ**
Horizontal	0.63°	0.61°	0.83	0.25	0.72°	0.64°	0.85	0.25	0.81°	0.96°	0.86	0.24
Vertical	0.64°	0.58°	0.84	0.24	0.77°	0.82°	0.85	0.24	0.87°	0.96°	0.85	0.25
Oblique	0.64°	0.60°	0.84	0.25	0.75°	0.73°	0.85	0.24	0.84°	0.96°	0.85	0.24

TABLE III
VELOCITY ACCURACY

	0 – 10° Amplitude				*0 – 15° Amplitude*				*All Saccades*			
	RMSE		**R^2**		**RMSE**		**R^2**		**RMSE**		**R^2**	
Component	**μ**	**σ**	**μ**	**σ**	**μ**	**σ**	**μ**	**σ**	**μ**	**σ**	**μ**	**σ**
Horizontal	98°/s	283°/s	0.47	0.29	103°/s	309°/s	0.49	0.29	116°/s	367°/s	0.51	0.29
Vertical	100°/s	287°/s	0.39	0.27	103°/s	272°/s	0.40	0.27	116°/s	333°/s	0.39	0.27
Oblique	118°/s	400°/s	0.55	0.26	124°/s	409°/s	0.59	0.25	141°/s	493°/s	0.59	0.25

Q. Estimation of Oculomotor Plant Characteristics (OPC)

The goal of the OPC estimation procedure is to derive a set of OPC values that allows for accurate simulation of recorded saccade trajectories. The procedure assumes that OPC are unique for each individual and are fixed within the individual.

To investigate the ability of the 2D-OP to simulate measured human saccade trajectories, an optimization problem was defined to reduce the sum of absolute positional error between a measured and simulated saccade. That is, Error = $\Sigma\ |m_i - s_i|$, where m_i is the measured position at a given time, i, and s_i is the simulated position produced by the 2D-OP model.

The following algorithm takes as an input all saccades recorded for a given individual and outputs a set of fixed OPC values for that individual. OPC for the horizontal and vertical trajectory of each saccade were optimized separately, and all model OPC were allowed to vary, these include (with initial values): K_{SE_AG} = 2.5, K_{SE_ANT} = 2.5, K_{LT_AG} = 1.2, K_{LT_ANT} = 1.2, N_{AG_C} = 0.8, N_{ANT_C} = 0.3, B_P = 0.06, B_{AG} = 0.046, B_{ANT} = 0.022, J = 0.000046, τ_{AG_AC} = 11.7, τ_{ANT_AC} = 2.4, τ_{AG_DE} = 2.0, τ_{ANT_DE} = 1.9, N_{FIX_C} = 14.0, N_{AG_SAC} = 100.0, N_{ANT_SAC} = 0.5, PW_{AG} for each component; where $K_P = N_{AG\_C} - N_{ANT\_C}$ in all relevant equations. Optimization was performed across all possible pulse widths within the duration of a given saccade using the Nelder-Mead (NM) simplex search algorithm [35] (MATLAB's fminsearch implementation) to minimize the absolute positional error between the measured and simulated trajectory; the pulse width with the least-error OPC set was selected for each saccade component. This resulted in the optimization of 18 OPC per component of

TABLE IV
MEASURED AND SIMULATED OBLIQUE MAIN SEQUENCES, $V_{PEAK} = V_{MAX}\,(1 - e^{-|Amplitude| / C})$

	0 – 10° Amplitude											
	Measured						**Simulated**					
	V_{MAX}		**C**		**R^2**		**V_{MAX}**		**C**		**R^2**	
Oblique Angle	**μ**	**σ**	**μ**	**σ**	**μ**	**σ**	**μ**	**σ**	**μ**	**σ**	**μ**	**σ**
0°	539	38	4.32	0.59	0.94	0.06	519	22	5.17	3.10	0.99	0.02
15°	553	149	4.71	1.90	0.88	0.15	634	212	6.08	3.65	0.94	0.15
30°	542	125	4.55	1.66	0.81	0.16	572	137	5.85	1.73	0.96	0.09
45°	587	118	5.22	2.43	0.85	0.19	649	159	6.10	2.00	0.97	0.04
60°	601	223	5.51	3.32	0.75	0.32	584	171	6.24	2.03	0.96	0.06
75°	563	125	4.37	2.34	0.78	0.23	575	160	6.93	4.89	0.96	0.04
90°	586	112	4.75	1.20	0.82	0.14	358	29	4.27	1.11	0.98	0.02
	0 – 15° Amplitude											
	Measured						**Simulated**					
	V_{MAX}		**C**		**R^2**		**V_{MAX}**		**C**		**R^2**	
Oblique Angle	**μ**	**σ**	**μ**	**σ**	**μ**	**σ**	**M**	**σ**	**μ**	**σ**	**μ**	**σ**
0°	597	128	5.37	1.92	0.79	0.25	630	156	9.33	2.94	0.94	0.07
15°	583	128	4.97	3.25	0.82	0.20	675	152	9.33	3.78	0.94	0.17
30°	627	129	5.38	2.32	0.84	0.14	654	161	8.01	3.17	0.95	0.05
45°	616	118	5.57	2.54	0.82	0.25	638	158	7.86	2.66	0.96	0.05
60°	590	175	4.99	2.79	0.59	0.38	579	150	7.19	2.37	0.95	0.06
75°	557	114	4.59	1.64	0.81	0.18	633	173	9.39	4.37	0.93	0.12
90°	619	149	6.28	2.43	0.78	0.20	611	319	8.06	5.26	0.99	0.01
	All Saccades											
	Measured						**Simulated**					
	V_{MAX}		**C**		**R^2**		**V_{MAX}**		**C**		**R^2**	
Oblique Angle	**μ**	**σ**	**μ**	**σ**	**μ**	**σ**	**μ**	**σ**	**μ**	**σ**	**μ**	**σ**
0°	584	108	5.56	1.65	0.82	0.24	633	121	10.38	3.43	0.95	0.07
15°	602	116	5.37	2.11	0.80	0.18	667	121	9.55	3.32	0.97	0.03
30°	625	95	5.94	3.05	0.84	0.14	649	155	8.28	3.26	0.95	0.05
45°	644	131	6.24	2.97	0.84	0.16	680	131	8.88	2.69	0.96	0.05
60°	615	179	5.16	2.71	0.59	0.35	606	165	8.81	3.79	0.94	0.09
75°	559	100	4.49	1.56	0.75	0.27	577	136	8.24	3.45	0.93	0.11
90°	624	152	6.33	2.52	0.76	0.20	447	91	6.03	1.73	0.89	0.23

each saccade, or 36 OPC to describe a given saccade within the 2D-OP.

This process was repeated in several stages, with certain OPC being fixed to their average least-error value at each stage, with the goal of stabilizing constants first (e.g. K_{SE}, K_{LT}, B_P, J, etc.), followed by equations (e.g. N_{AG_SAC}, PW, etc.) ordered by increasing complexity. The output from each stage is provided as an input to the subsequent stage. At each stage, fixing certain OPC results in the formation of more stable and noticeable patterns in the values of the remaining OPC, allowing more accuracy in the resulting optimization and subsequent regression of parameter values. Several optimization techniques were considered and the heuristic presented in Figure 3 was selected because it produced OPC that allow the 2D-OP to simulate more accurate trajectories.

This process was repeated on sub-intervals of 0-10° and 0-15° amplitude, to assess the ability of the 2D-OP to model saccades within a reduced range.

R. Comparison Metrics

In comparing the saccades simulated by the 2D-OP to measured (or expected) values, the following metrics were employed, where m indicates a measured/expected value, p indicates a predicted/simulated value, and n denotes the total number of data points being compared:

$$RMSE = \frac{\sqrt{\sum(m-p)^2}}{n} \quad \textbf{(45)}$$

$$R^2 = \frac{(n\sum(m \times p) - \sum(m)\sum(p))^2}{(n\sum(m^2) - (\sum(m))^2)(n\sum(p^2) - (\sum(p))^2)} \quad \textbf{(46)}$$

V. RESULTS

S. Simulation Results

Table I presents averaged OPC parameters across all subjects, Table II presents the accuracy results of the OPC estimation experiment, specifically the RMSE of the measured vs. simulated saccade trajectories, and the R^2 correlation between the measured and simulated saccade trajectories, Table III presents the accuracy of the simulated vectorial velocity, similar to Table II, and Table IV gives the average main sequence equations for the various oblique angles and the corresponding R^2 of the regression. Figures 3-5 show examples of measured and simulated main sequences from several subjects. Each line in those figures represents a different oblique angle of movement. Figures 6-7 presents examples of measured and simulated trajectories for the oblique saccades. Figures 9-11 present corresponding velocity profiles.

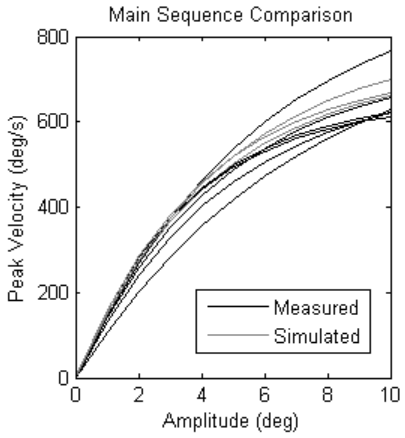

Figure 3. 0 – 10° amplitude, oblique main sequence, subject 8.

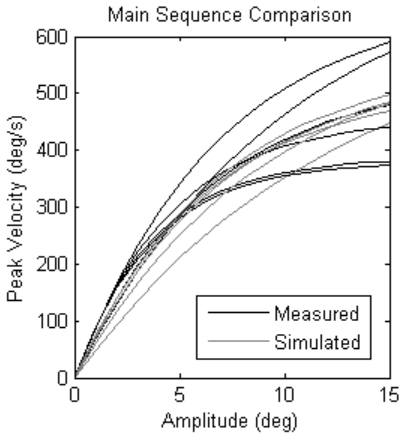

Figure 4. 0 – 15° amplitude, oblique main sequence, subject 24.

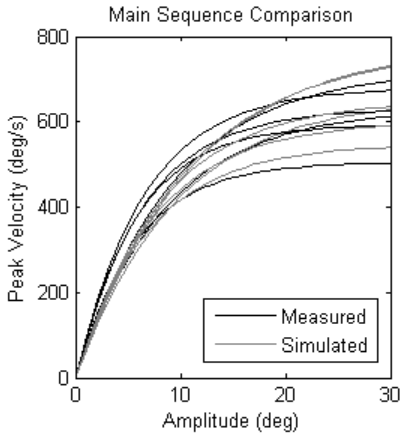

Figure 5. All saccades, oblique main sequence, subject 24.

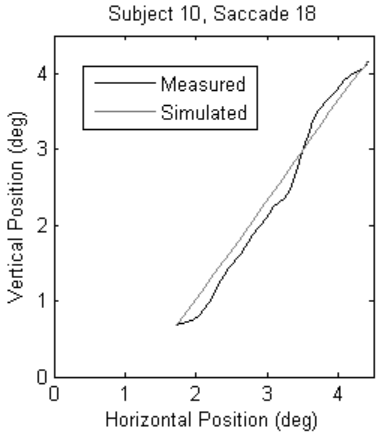

Figure 6. Comparative trajectory of a 3° saccade at a 45° angle.

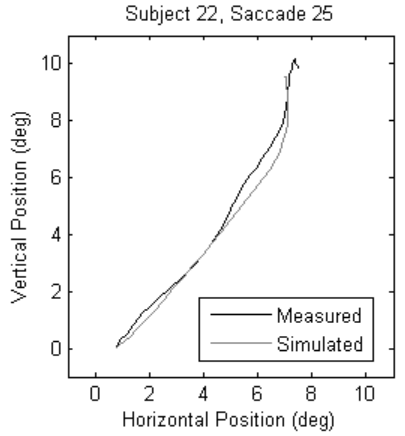

Figure 7. Comparative trajectory of a 12° saccade at a 60° angle.

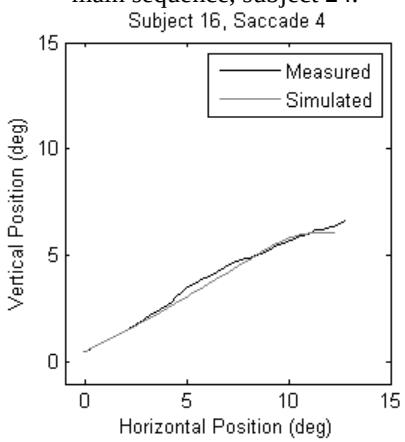

Figure 8. Comparative trajectory of a 15° saccade at a 30° angle.

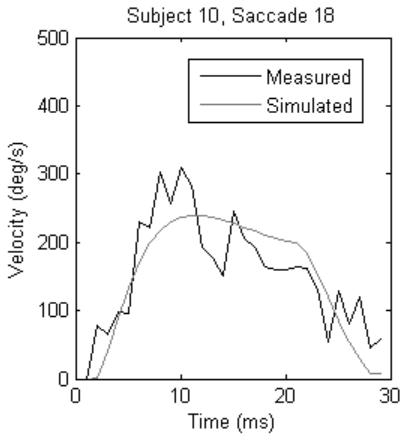

Figure 9. Comparative velocity of a 3° saccade at a 45° angle.

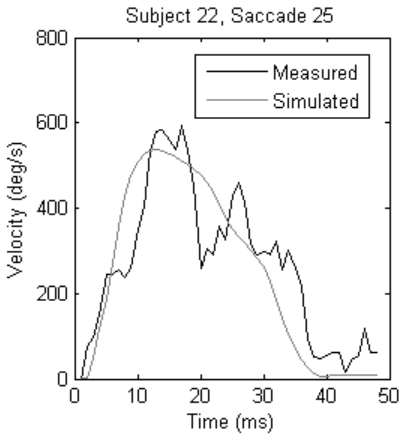

Figure 10. Comparative velocity of a 12° saccade at a 60° angle.

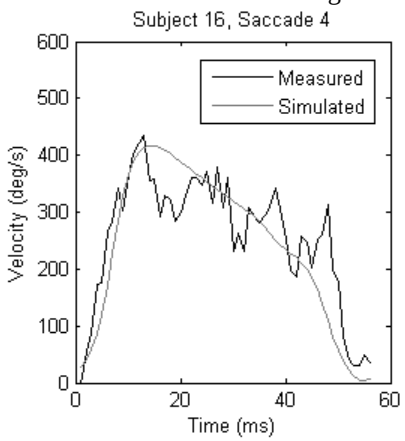

Figure 11. Comparative velocity of a 15° saccade at a 30° angle.

T. Estimated Oculomotor Plant Characteristics

With the exception of N_{AG_SAC}, obtained OPC values are relatively consistent across the considered intervals (generally varying by less than 10% in both μ and σ) and fall within a degree of magnitude from their initial generic values.

U. Accuracy of Simulated Saccades

The results indicate that positional error was small (0.63-0.87° on average). As the range of saccades included in the OPC estimation of a given subject increases, both the RMSE and R^2 of the simulated trajectory increases. That is, as the data set increases, the average positional error of simulated saccades across that data set increases, but the average correlation between measured and simulated saccades also increases. This is likely due to the inclusion of greater

amplitude saccades in subsequent data sets, where larger saccades contribute relatively more error to the RMSE calculation. Such error might occur due to the linear representation of the OP by the 2D-OP model, as the linear representation is more accurate toward primary eye position.

The results are similar to that of the positional accuracy, as the range of saccades included in OPC estimation increases, both the RMSE and R^2 of the simulated velocity increase. It should also be noted, that across all saccades the ratio of peak velocity to average velocity (Q) of measured saccades had an average value of 2.74 (SD = 3.02), while the simulated Q had an average value of 2.01 (SD = 0.66).

V. Measured & Simulated Oblique Main Sequences

The main sequence relationship for the oblique angles of each subject was calculated separately based on the available data for both measured and simulated saccades. In some cases, insufficient data points for a given angle and outliers resulted in unusable fits. To mediate the effect of including this data in the average, relationships were excluded based on the following criteria: if regression failed for a given data set, the R^2 of the regression was negative, or the value of V_{MAX} was unrealistically high (>1000 deg/s), the relationship was excluded from the averaged relationship values. Because of this exclusion, the averaged value for each angle was not necessarily drawn from the average data across all subjects, but only a subset of this. Of the oblique angles, 0° and 90° tended to have the most data loss in this respect. The explanation being that purely horizontal/vertical saccades are very rare, and even when the eye is programmed for such a saccade, there is a certain amount of drift that occurs in the orthogonal component, resulting in a skewed oblique angle.

As expected from the literature [1, 18, 19, 22, 23], the simulated values of V_{MAX} produced for all angles (358 ~ 680 deg/s) are within a realistic range (400 ~ 800 deg/s), as is the curvature C in Equation (1). The average R^2 for regressions of measured saccade data are often lower than the average R^2 for simulated saccade data, suggesting that the model provides a stricter adherence to the main sequence relationship than is found in normal human saccade data (possibly due to noise or measurement accuracy).

VI. DISCUSSION

W. Evaluation Limitations

The 2D-OP is able to simulate saccades from any point to any point in a two-dimensional plane; however, the evaluation of the 2D-OP was performed only for centrifugal saccades in the first quadrant that originated from at or near the primary eye position. This simplification was necessary to establish a thorough baseline for the accuracy of the 2D-OP. Other types of oblique saccades might require adjustments to the parameters responsible for generating the neuronal control signal, and will require some mechanism to incorporate the information about the coordinates of onset/offset position in addition to saccade amplitude. Additional research is required to establish those strategies.

X. 2D-OP Simplifications

The 2D-OP is not an exact replica of the human oculomotor plant. 1) The 2D-OP employs a linear representation of the major anatomical components, which in real systems are non-linear [36]. 2) The 2D-OP does not explicitly account for the effects of the superior and inferior obliques, primarily responsible for extorsion/intorsion of the eye globe. 3) The 2D-OP models rotations as translations, which is acceptable for saccades to secondary positions, but neglects the non-commutativity of rotations when modeling saccades to tertiary positions. Considering the simplifications, the results presented by Tables II-IV indicate that the 2D-OP is able to simulate centrifugal oblique saccades with properties resembling those produced by normal humans.

Y. Practical Advantages & Applications of the 2D-OP

The 2D-OP, however simplified, represents the major anatomical components of the OP. The simple pulse-step form of the neuronal control signal allows simulation of saccade trajectories in cases when the onset and offset coordinates are provided to the model with the equations responsible for pulse height (Equation (14)) and pulse width (Equation (11)) computation. The 2D-OP can be represented as separate 1D-OP models for each component of movement, reducing the amount of computations done by up to 4 times and allowing parallel computation of each component.

Practical applications of the 2D-OP might include: 1) biometric systems, in which individual anatomical components represented in the 2D-OP allow for the unique identification of individuals [37]; 2) human-computer interaction, in which simulated saccadic trajectories allow research into the properties of the eye movement signal, providing capabilities for developing extremely fast target selection methods, where selection occurs at saccade onset [38]; 3) usability, in which individual EOM forces can be approximated by the 2D-OP, providing an opportunity to estimate the physical effort exerted by a user during a specific task [39]; 4) eye tracking, in which the linear design of the 2D-OP allows its encapsulation in Kalman filter form, providing the means for robust signal recovery and noise reducing facilities [7], and saccade trajectory prediction for gaze-contingent compression [40].

VII. CONCLUSION

This paper has presented a two-dimensional linear homeomorphic model (2D-OP) of the oculomotor plant driven by a simplified pulse-step neuronal control signal. An optimization algorithm was developed that estimates the characteristics of the oculomotor plant as represented by the 2D-OP from the recorded eye movement signal of an individual.

To assess performance of the 2D-OP, approximately 1040 centrifugal oblique saccades were recorded from 30 humans. The results suggest that the 2D-OP driven by person-specific oculomotor plant characteristics is capable of simulating saccadic eye movements with characteristics

resembling those of normal humans. The most accurate simulation results were obtained for the saccades with amplitudes of up to 10°, however even larger saccades were simulated relatively accurately with average positional and velocity error not exceeding 0.87° and 141°/s respectively. Oblique main sequences generated by the 2D-OP resulted in a better fit to the stereotyped exponential form than the recorded human data.

The presented 2D-OP model can be simplified into two smaller one-dimensional models that produce identical simulation results but considerably speed up the simulation process. The practical applications of such a model might include: enhanced security in biometric identification systems; improved noise reduction and signal recovery facilities for eye tracking systems; and additional metrics from which to determine user effort during usability testing.

VIII. ACKNOWLEDGEMENTS

The work was partially funded by grant from the National Institute of Standards #60NANB10D213. Special gratitude is expressed to Dr. Alex Karpov for his assistance with data collection and processing, and Dr. Christian Quaia for his comments and suggestions.

IX. REFERENCES

[1] R. J. Leigh and D. S. Zee, *The Neurology of Eye Movements*, 4 ed.: Oxford University Press, USA, 2006.

[2] J. D. Crawford, *et al.*, "Neural control of three-dimensional eye and head movements," *Current Opinion in Neurobiology*, vol. 13, pp. 655-662, 2003.

[3] G. Westheimer, "Mechanism of saccadic eye movements," *AMA Arch Ophthalmol*, vol. 52, pp. 710-724, November 1, 1954 1954.

[4] D. A. Robinson, "Models of the saccadic eye movement control system," *Biological Cybernetics*, vol. 14, pp. 71-83, 1973.

[5] M. R. Clark and L. Stark, "Control of human eye movements: I. Modelling of extraocular muscles; II. A model for the extraocular plant mechanism; III. Dynamic characteristics of the eye tracking mechanism," *Mathematical Biosciences*, vol. 20, pp. 91-265, 1974.

[6] A. T. Bahill, "Development, validation and sensitivity analyses of human eye movement models," *CRC Critical Reviews in Bioengineering*, vol. 4, pp. 311-355, 1980.

[7] O. V. Komogortsev and J. I. Khan, "Eye movement prediction by Kalman filter with integrated linear horizontal oculomotor plant mechanical model," presented at the Proceedings of the 2008 symposium on Eye tracking research & applications, Savannah, Georgia, 2008.

[8] O. Komogortsev and J. Khan, "Eye movement prediction by oculomotor plant Kalman filter with brainstem control," *Journal of Control Theory and Applications*, vol. 7, pp. 14-22, 2009.

[9] J. D. Enderle and W. Zhou, *Models of Horizontal Eye Movements, Part 2: A 3rd-Order Linear Saccade Model*: Morgan and Claypool Publishers, 2010.

[10] C. F. Martin and L. Schovanec, "Muscle mechanics and dynamics of ocular motion," *Journal of Mathematical Systems Estimation and Control*, vol. 8, pp. 233-236, 1998.

[11] D. Tweed, "Three-Dimensional Model of the Human Eye-Head Saccadic System," *Journal of Neurophysiology*, vol. 77, pp. 654-666, February 1, 1997 1997.

[12] C. Quaia and L. M. Optican, "Commutative Saccadic Generator is Sufficient to Control a 3-D Ocular Plant With Pulleys," *Journal of Neurophysiology*, vol. 79, pp. 3197-3215, 1998.

[13] T. Raphan, "Modeling control of eye orientation in three dimensions. I. Role of muscle pulleys in determining saccadic trajectory," *Journal of Neurophysiology*, vol. 79, pp. 2653-1667, 1998.

[14] P. Lockwood-Cooke, *et al.*, "A dynamic 3-D model of ocular motion," presented at the IEEE Conference on Decision and Control, 1999.

[15] A. D. Polpitiya and B. K. Ghosh, "Modelling and control of eye-movement with musculotendon dynamics," in *American Control Conference*, 2002, pp. 2313-2318.

[16] C. Quaia and L. M. Optican, "Dynamic eye plant models and the control of eye movements," *Strabismus*, vol. 11, pp. 17-31, 2003.

[17] R. H. Carpenter, *Movements of the eyes*: Pion (London), 1977.

[18] A. T. Bahill, *et al.*, "The main sequence, a tool for studying human eye movements," *Mathematical Biosciences*, vol. 24, pp. 191-204, 1975.

[19] A. C. Smit, *et al.*, "Component stretching in fast and slow oblique saccades in the human," *Experimental Brain Research*, vol. 81, pp. 325-334, 1990.

[20] S. Jayarathna and O. V. Komogortsev, "2D Oculomotor Plant Mathematical Model for eye movement simulation," presented at the 8th IEEE International Conference on BioInformatics and BioEngineering, 2008.

[21] D. R. Wilkie, "Muscle," *Studies in Biology*, vol. 11, 1976.

[22] F. Fioravanti, *et al.*, "Saccadic eye movement conjugation in children," *Vision Research*, vol. 35, pp. 3217-3228, 1995.

[23] A. G. Huaman and J. A. Sharpe, "Vertical saccades in senescence," *Investigative Ophthalmology & Visual Science*, vol. 34, pp. 2588-95, July 1, 1993 1993.

[24] R. D. Yee, *et al.*, "Velocities of vertical saccades with different eye movement recording methods," *Investigative Ophthalmology & Visual Science*, vol. 26, pp. 938-44, July 1, 1985 1985.

[25] D. Pelisson and C. Prablanc, "Kinematics of centrifugal and centripetal saccadic eye movements in man," *Vision Research*, vol. 28, pp. 87-94, 1988.

[26] A. T. Bahill and L. Stark, "Oblique saccadic eye movements. Independence of horizontal and vertical channels.," *Archives of Ophthalmology*, vol. 95, pp. 1258-1261, 1977.

[27] G. E. Grossman and D. A. Robinson, "Ambivalence in modelling oblique saccades," *Biological Cybernetics*, vol. 58, pp. 13-18, 1988.

[28] O. V. Komogortsev, *et al.*, "2D Oculomotor Plant Mathematical Model for Eye Movement Simulation," ed, 2011.

[29] O. V. Komogortsev, "Eye Movement Prediction by Oculomotor Plant Modeling with Kalman Filter," Ph.D., Computer Science, Kent State University, Kent, OH, 2007.

[30] D. L. Sparks, "The brainstem control of saccadic eye movements," *Nat Rev Neurosci*, vol. 3, pp. 952-964, 2002.

[31] H. P. Goldstein and D. A. Robinson, "Hysteresis and slow drift in abducens unit activity," *Journal of Neurophysiology*, vol. 55, pp. 1044-1056, May 1, 1986 1986.

[32] L. M. Optican and F. A. Miles, "Visually induced adaptive changes in primate saccadic oculomotor control signals," *Journal of Neurophysiology*, vol. 54, pp. 940-958, October 1, 1985 1985.

[33] EyeLink. (2010). *EyeLink II*. Available: http://www.sr-research.com/EL_1000.html

[34] O. V. Komogortsev, *et al.*, "Standardization of Automated Analyses of Oculomotor Fixation and Saccadic Behaviors," *IEEE Transactions on Biomedical Engineering*, vol. 57, pp. 2635-2645, 2010.

[35] J. C. Lagarias, *et al.*, "Convergence Properties of the Nelder--Mead Simplex Method in Low Dimensions," *SIAM Journal on Optimization*, vol. 9, pp. 112-147, 1998.

[36] C. Quaia, *et al.*, "The Viscoelastic Properties of Passive Eye Muscle in Primates. III: Force Elicited by Natural Elongations," *PLoS ONE*, vol. 5, p. e9595, 2010.

[37] O. V. Komogortsev, *et al.*, "Biometric identification via an oculomotor plant mathematical model," in *Proceedings of the 2010 Symposium on Eye-Tracking Research & Applications*, Austin, Texas, 2010, pp. 57-60.

[38] O. V. Komogortsev, *et al.*, "Instantaneous Saccade Driven Eye Gaze Interaction," in *ACM International Conference on Advances in Computer Entertainment Technology*, 2009 pp. 1-8.

[39] O. Komogortsev, *et al.*, "An Effort Based Model of Software Usability," presented at the International Conference on Software Engineering Theory and Practice (SETP), Orlando, FL, 2009.

[40] O. V. Komogortsev, "Gaze-contingent video compression with targeted gaze containment performance," *Journal of Electronic Imaging*, vol. 18, pp. 033001-10, 2009.